Giant Reversible Piezoelectricity from Symmetry-Governed Stochastic Dipole Hopping

Denan Li,[1,2] Haofei Ni,[3] Yi Zhang,[3] and Shi Liu[2,4,*]
[1]Fudan University, Shanghai 200433, China
[2]Department of Physics, School of Science, Westlake University, Hangzhou 310030, China
[3]Institute for Science and Applications of Molecular Ferroelectrics, Key Laboratory of the Ministry of Education for Advanced Catalysis Materials, Zhejiang Normal University, Jinhua, Zhejiang 321004, China
[4]Institute of Natural Sciences, Westlake Institute for Advanced Study, Hangzhou 310024, China

(Received 21 July 2025; accepted 12 December 2025; published 2 January 2026)

Organic-inorganic hybrid perovskites with giant piezoelectric responses, exemplified by TMCM-$CdCl_3$, represent a promising platform for flexible and environmentally friendly electromechanical materials. However, the microscopic origin of such exceptional performance in this weakly polar system has remained elusive. Here, using deep-learning-assisted large-scale molecular dynamics simulations, we resolve this paradox by reproducing a giant piezoelectric coefficient of ≈211 pC/N and demonstrating that it arises from the collective contribution of multiple intrinsic components, particularly the shear component d_{15}. This effect does not stem from conventional polarization rotation or phase switching, but instead originates from stochastic 120° in-plane rotational hopping of a small fraction of organic cations. This discrete hopping mechanism is governed by the local C_3-symmetric halogen-bonding network between the host framework and the guest cation. The Arrhenius-type temperature dependence of d_{15} further confirms the role of thermally activated dipole hopping. This Letter provides a clear pathway to enhance piezoelectric performance of hybrid materials through rational engineering of host-guest interactions.

DOI: 10.1103/vxdj-zpy3

Piezoelectric materials, which can convert mechanical energy into electrical energy and vice versa, are foundational to a wide range of modern technologies [1]. For decades, this technological landscape has been dominated by inorganic ferroelectrics such as barium titanate (BTO) and lead zirconate titanate (PZT) [2–6]. While robust in performance, these materials are heavy, brittle, require high-temperature processing, and often contain toxic elements, making them unsuitable for emerging applications that demand flexible, lightweight, and biocompatible piezoelectrics. This has driven a search for molecular alternatives, which promise mechanical flexibility and environmentally friendly solution processability but have historically been limited by a fundamental trade-off: molecular ferroelectrics tend to exhibit low spontaneous polarization, leading to weak piezoelectric response [7–11].

The discovery of the hybrid organic-inorganic ferroelectric perovskite trimethylchloromethyl ammonium trichlorocadmium(II) [$Me_3NCH_2ClCdCl_3$, (TMCM-$CdCl_3$)], composed of organic $TMCM^+$ cations and inorganic $CdCl_3^-$ frameworks and adopting the $BaNiO_3$-like perovskite structure, marks an important advancement for developing flexible, low-temperature-processable piezoelectric materials [12]. However, it also presents a fundamental paradox: despite having a spontaneous polarization of only $4-5\ \mu C/cm^2$, an order of magnitude smaller than that of BTO (≈25 $\mu C/cm^2$), TMCM-$CdCl_3$ achieves a piezoelectric strain coefficient of $d_{33} \approx 220$ pC/N [12], comparable to BTO [13]. The striking anomaly of a weakly polar material exhibiting a giant piezoelectric response suggests the presence of an unconventional physical mechanism.

Two primary theories have been proposed to resolve the paradox. The original study of TMCM-based perovskites suggested a ferroelastic polarization rotation mechanism [12]. Crystallographic and vector piezoresponse force microscopy analyses revealed that monoclinic TMCM-$CdCl_3$ hosts twelve energetically equivalent polar states. It was argued that applied stress could trigger ferroelastic switching between these states, causing a large-angle reorientation of the polarization vector and a giant piezoelectric response. A key limitation of this theory is that reversible ferroelastic switching, essential for reversible piezoelectricity, often requires alternating compressive and tensile stress, a condition not typically met during standard unipolar piezoelectric measurements. A later theoretical study proposed a phase-switching mechanism [14]. First-principles calculations identified a metastable phase featuring $TMCM^+$ cations in head-to-head and tail-to-tail orientations. The piezoelectric response was attributed to a stress-induced transition between this phase and the ground-state monoclinic structure. This theory was based on static, zero-Kelvin unit-cell calculations that neglected thermal fluctuations and molecular dipole

*Contact author: liushi@westlake.edu.cn

dynamics, factors likely crucial to understanding the experimental behavior at finite temperatures.

Here, we resolve this long-standing puzzle using large-scale molecular dynamics (MD) simulations of TMCM-$CdCl_3$, enabled by a high-fidelity machine-learning force field trained exclusively on first-principles data. By computing the full piezoelectric tensor in the single-domain limit at 300 K, we show that the experimentally observed giant response is dominated not by the intrinsic longitudinal coefficient d_{33}, but by large shear components, particularly $d_{15} = 163$ pC/N. Notably, applying a proper tensor transformation from the crystal to the laboratory frame yields an effective d_{33}^{eff} of 211 pC/N at 300 K, closely matching the experimental value of 220 pC/N. We uncover a novel piezoelectric mechanism distinct from both ferroelastic and phase switching: a stress-driven, thermally activated stochastic 120° rotational hopping of a small fraction of $TMCM^+$ cations. This hopping is governed by the local C_3 symmetry imposed by the halogen bonds between organic cations and the inorganic framework. When the fraction of hopped cations remains below a critical threshold, they can return to their original states once the stress is removed, exhibiting a shape-memory-like effect. This collective dipole hopping is further supported by the strong temperature dependence of the piezoelectric response. Finally, we distinguish this useful, reversible behavior from the irreversible, large-strain ferroelastic switching that defines the material's fatigue limit.

Previous studies have shown that TMCM-$CdCl_3$ crystallizes in the monoclinic space group Cc in the ferroelectric phase and the hexagonal space group $P6_3/mmc$ in the paraelectric phase. We introduce an intuitive host-guest framework to clarify the connection between the orientations of $TMCM^+$ cations and the macroscopic polarization [14–16]. As depicted in Fig. 1(a), one-dimensional $CdCl_3^-$ chains, the "host," self-assemble into a triangular lattice, forming triangular channels along the [001] direction. The functional "guests" are $TMCM^+$ cations, which reside within these channels and form their own A-B stacked triangular sublattices. In the paraelectric phase, molecular cations are fully disordered, yielding a primitive hexagonal unit cell. The ferroelectric phase features alignment of the out-of-plane components of all molecular dipoles [Fig. 1(b)]. While dipoles within each layer are aligned, adjacent layers of dipoles are not fully coaligned, as seen in the side [Fig. 1(b)] and top-down views [Fig. 1(c)]. We find

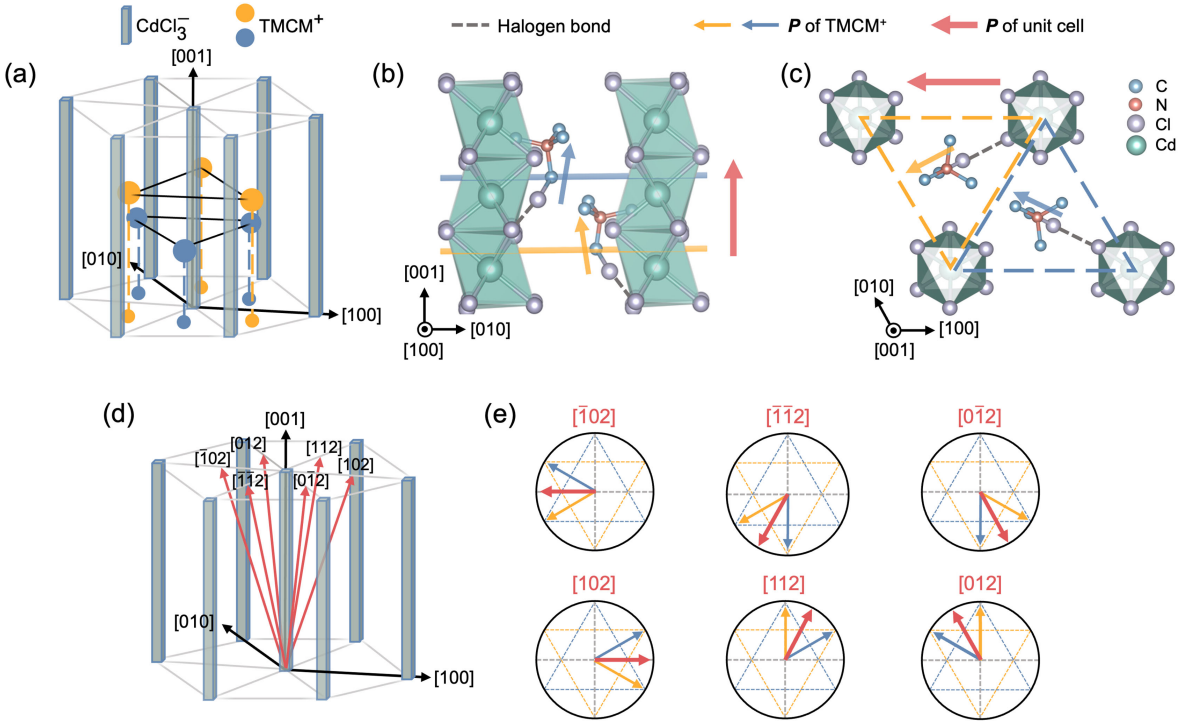

FIG. 1. Crystal structure and polarization variants of TMCM-$CdCl_3$. (a) Schematic illustration of the host-guest framework. One-dimensional inorganic $CdCl_3^-$ chains form a triangular lattice with organic $TMCM^+$ cations occupying the interstitial sites to create A–B stacked triangular sublattices. The crystallographic axes and directions shown are defined with respect to the paraelectric hexagonal lattice. (b) Side view and (c) top view of the crystal structure in the ferroelectric phase. The dashed triangle indicates the local triple-well potential energy surface associated with the in-plane rotation of a $TMCM^+$ cation. In this phase, molecules are anchored by highly directional $CH_2 - Cl \cdots Cl$ halogen bonds (gray dashed lines). Due to the helical arrangement of Cl atoms along the $CdCl_3^-$ chain, the molecular dipoles in adjacent layers are not fully aligned. (d) Six equivalent macroscopic polarization directions in the ferroelectric phase, each with different in-plane components. (e) Schematics showing the collective in-plane orientations of molecular dipoles corresponding to the six polar variants in (d). Yellow and blue triangles represent the two dipole layers within the unit cell as shown in (b) and (c), and red arrows denote the net in-plane polarization.

that the orientation of each $TMCM^+$ cation is anchored by highly directional $CH_2-Cl\cdots Cl$ halogen bonds [dashed lines in Figs. 1(b) and 1(c)], which act as a "molecular lock" connecting the guest cation to the surrounding inorganic chains. Additionally, the Cl atom arrangement along the chains prevents full dipole alignment across layers. Due to the C_3 symmetry of each $CdCl_3^-$ chain along [001], the cation is restricted to one of three equivalent orientations with its in-plane dipole directed toward a triangular channel edge. This symmetry gives rise to a C_3-symmetric potential energy landscape for coherent switching (see Supplemental Material, Fig. S1 [17]). Since the unit cell of the ferroelectric phase contains two layers of molecular dipoles, the in-plane polarization can be intuitively understood using the schematic in Fig. 1(e), where each dipole layer is represented by a triangle, with the two triangles rotated 180° to reflect the stacking arrangement. The six macroscopic polar variants along [102] and equivalent directions [Fig. 1(d)] correspond to distinct combinations of allowed relative orientations between the two $TMCM^+$ layers within the unit cell.

Theoretical prediction of finite-temperature piezoelectric coefficients in hybrid materials such as TMCM-$CdCl_3$ is challenging, as conventional approaches such as density functional perturbation theory often yield negligible values [14,36]. This limitation likely arises from the neglect of thermal fluctuations and the associated order-disorder behavior of molecular dipoles. To overcome this challenge, we developed a deep neural network-based interatomic potential (deep potential [37,38]), which enables large-scale MD simulations of TMCM-$CdCl_3$ at finite temperatures. It can also directly predict total polarization from atomic positions. Our model demonstrates high fidelity across a wide range of validation tests. It achieves an excellent fit to the reference DFT database, with low mean absolute errors for energy (0.214 meV/atom), force (0.017 eV/Å), virial (1.609 meV/atom), and polarization (0.06 $\mu C/cm^2$) and the polarization change response to structural evolution (see Supplemental Material, Sec. V [17]). The training database, final trained model, and representative input files are publicly available [39]. Additional model validation details are provided in the Supplemental Material [17]. The piezoelectric tensor element is calculated as $d_{ij}=\Delta P_i/\sigma_j$, reflecting the polarization change along direction $i\,(\Delta P_i)$ due to an applied stress with component j (σ_j in Voigt notation).

We now detail the calculation of d_{15} (with indices defined relative to the monoclinic unit cell). A shear deformation is imposed by varying the lattice angle β by an amount $\Delta\beta$ [Fig. 2(a) inset] while allowing all other lattice parameters to fully relax during finite-temperature MD simulations with β held fixed, using a 10 800-atom supercell. At equilibrium, only the shear stress component σ_5 is nonzero, establishing a one-to-one relationship among $\Delta\beta$, σ_5, and P_1. Figure 2 shows the evolution of P_1 and σ_5 with $\Delta\beta$ at 300 K, along with dipole density plots illustrating the distributions of in-plane molecular dipole orientations. The starting polar state I has in-plane polarization along $[\bar{1}00]$ ($P_1\approx -4\ \mu C/cm^2$). As shear strain increases, the shear stress σ_5 increases in magnitude, while all other stress components (σ_j, $j\neq 5$) remain negligible [Fig. 2(b)], confirming mechanical equilibrium under fixed $\Delta\beta$, with σ_5 balancing the imposed deformation. Dipole density plots [Fig. 2(f)] reveal that in strained state II, dipoles reorient nonuniformly: a subset undergoes 120° hops into adjacent symmetry-equivalent potential wells, forming localized "orientational defects" within the original domain [16].

Notably, the shear stress σ_5 reaches a maximum value σ_5^t at a critical shear deformation $\Delta\beta^t\approx 2.8°$, marking the threshold for piezoelectric reversibility. State II lies just below this threshold. When the stress is removed, the system relaxes to state II′ [see Fig. 2(f)], nearly identical to the initial state I. This indicates that dipoles return to their original orientations via reverse 120° hopping, yielding a fully reversible piezoelectric response. In contrast, when $\Delta\beta>\Delta\beta^t$, the system transitions to a fundamentally different configuration, represented by state III, characterized by a more isotropic distribution of in-plane dipole orientations. After unloading, it relaxes to state III′, where dipoles occupy four symmetry-related wells, clearly distinct from state I. These results demonstrate that σ_5^t associated with $\Delta\beta^t$ defines the limit for reversible piezoelectric switching. We thus define the reversible shear piezoelectric coefficient using the secant modulus, $d_{15}=\Delta P_1^t/\sigma_5^t=163$ pC/N, which provides a balanced figure of merit for this highly nonlinear system, averaging the response across the full reversible range and avoiding both the underestimation of the low-stress regime and the overestimation of the high-stress, precritical regime. It is noted that the strained state with $\Delta\beta^t$ can be stabilized by applying a constant shear stress in NPT simulations (see Supplemental Material, Sec. VII [17]). More precisely, it represents a stress-induced stable configuration that precedes the true critical point. The estimated theoretical d_{15} thus serves as an approximated theoretical limit, while the giant response remains robust. Similarly, we find that $d_{24}=-135$ pC/N, computed using the same method, also results from the stochastic in-plane hopping of molecular dipoles (see Supplemental Material, Sec. VIII [17]).

Table I presents the intrinsic piezoelectric tensor calculated in the single-crystal, single-domain limit at 300 K using the method described above. Interestingly, the longitudinal component d_{33} is low at 14 pC/N. This indicates that stress applied along the c-axis induces minimal polarization change, reflecting the structural rigidity of the $CdCl_3^-$ inorganic chains. The components $d_{15}=163$ pC/N and $d_{11}=77$ pC/N are significantly larger.

In piezoelectric coefficient measurements, the applied stress σ^Z (along the film-normal, laboratory Z-axis) does not necessarily align with the crystallographic axes. As a result, the effective coefficient measured along Z, d_{33}^{eff}, can

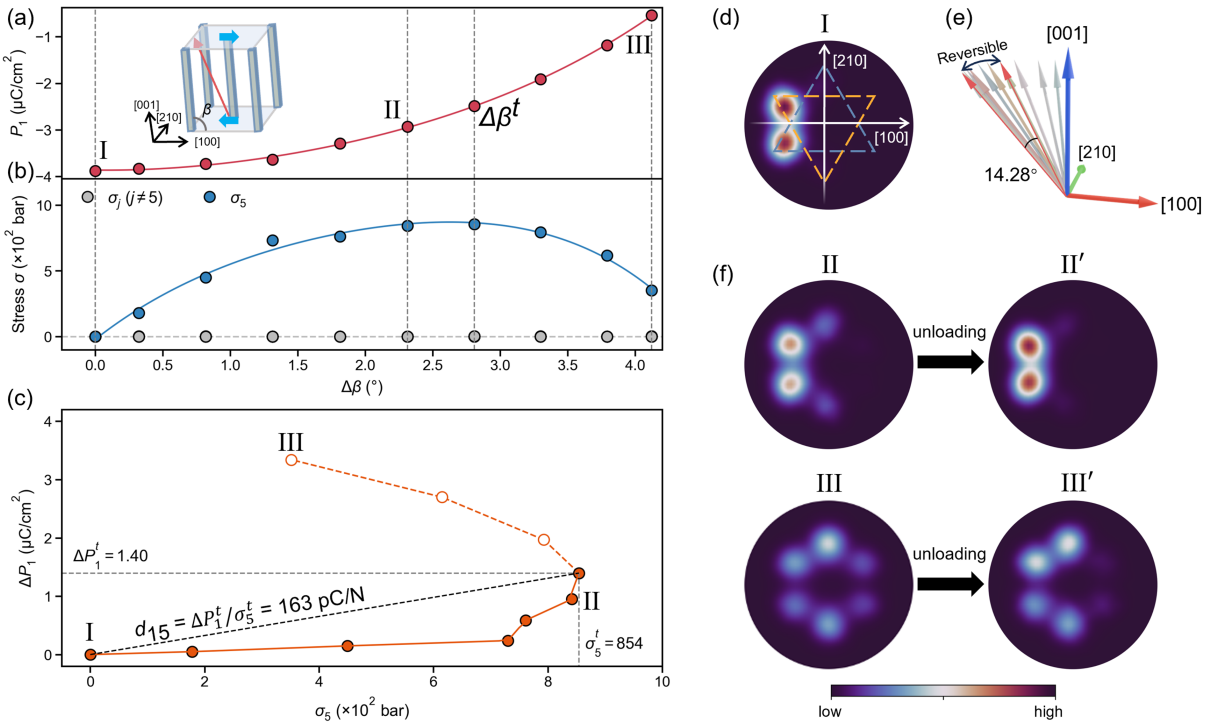

FIG. 2. Shear stress-induced reversible giant piezoelectric response via molecular dipole hopping. (a) Evolution of the polarization component along [100], P_1, and (b) shear stress σ_5 as a function of shear strain $\Delta\beta$. The inset in (a) illustrates the initial state I, characterized by a monoclinic unit cell with in-plane polarization aligned along [$\bar{1}$00]. The shear strain is imposed by varying the lattice angle β while allowing all other lattice parameters to relax. MD simulations ensure that for a fixed $\Delta\beta$, all other stress components (σ_j, $j \neq 5$) remain negligible, as confirmed in (b). The shear stress σ_5 reaches a maximum at a critical strain $\Delta\beta^t$. (c) Polarization change ΔP_1 as a function of σ_5, derived from (a) and (b). (d) In-plane dipole orientation density plot for $TMCM^+$ cations in the initial state I, following the schematic in Fig. 1. (e) Reversible region for the rotation of the macroscopic polarization. $\Delta\beta_t$ corresponds to a small rotational angle of 14.28°. (f) Dipole orientation density plots for strained states II and III and their corresponding relaxed configurations after unloading (II′ and III′). The transition between states I and II is reversible, while the transition from I to III is irreversible, as III′ is different from I.

reflect a combination of multiple components of the intrinsic piezoelectric tensor. To quantitatively relate the intrinsic tensor to d_{33}^{eff}, we perform a tensor rotation to determine the orientation of σ^Z that maximizes the response. We find that d_{33}^{eff} reaches 211 pC/N when σ^Z is nearly orthogonal to the polarization vector (see rotation matrix in Fig. S14 [17]), in excellent agreement with the experimental value of 220 pC/N. This optimal σ^Z direction is close to [102], also consistent with experimental observations that the maximum response is obtained near this crystallographic direction [12]. The origin of the enhanced effective response, exceeding that of any single intrinsic component, can be understood as follows. Because the polarization vector of $TMCM\text{-}CdCl_3$ does not align with the unit cell's crystallographic axes, σ^Z projects onto multiple stress components in the crystal frame: $\sigma^Z = 0.64\sigma_1 + 0.36\sigma_3 + 0.48\sigma_5$ (see derivations in Fig. S14 [17]). Consequently, the effective response combines contributions from several intrinsic tensor elements, specifically d_{11}, d_{13}, d_{15}, d_{31}, d_{33}, and d_{35}, which collectively yield the giant piezoelectric response of 211 pC/N. Among them, d_{15} and d_{11} account for about 59% and 18% of d_{33}^{eff}, respectively.

The excellent agreement between theory and experiment validates our finite-temperature MD-based approach, which further reveals the microscopic origin of the giant response. The piezoelectric response of $TMCM\text{-}CdCl_3$ primarily arises

TABLE I. Intrinsic piezoelectric strain tensor (in pC/N) calculated from MD simulations in the crystal frame and the effective piezoelectric strain tensor (d^{eff}) in the laboratory frame, both presented in matrix form. The largest component is highlighted in bold.

d_{ij}						Crystal frame (intrinsic)						Laboratory frame (d^{eff})					
d_{11}	d_{12}	d_{13}	d_{14}	d_{15}	d_{16}	77	54	27	40	**163**	−1	−47	23	78	12	−7	−16
d_{21}	d_{22}	d_{23}	d_{24}	d_{25}	d_{26}	−15	−37	−14	−135	16	31	−30	−37	0	−92	−5	100
d_{31}	d_{32}	d_{33}	d_{34}	d_{35}	d_{36}	25	11	14	5	45	0	−104	49	**211**	20	−22	−28

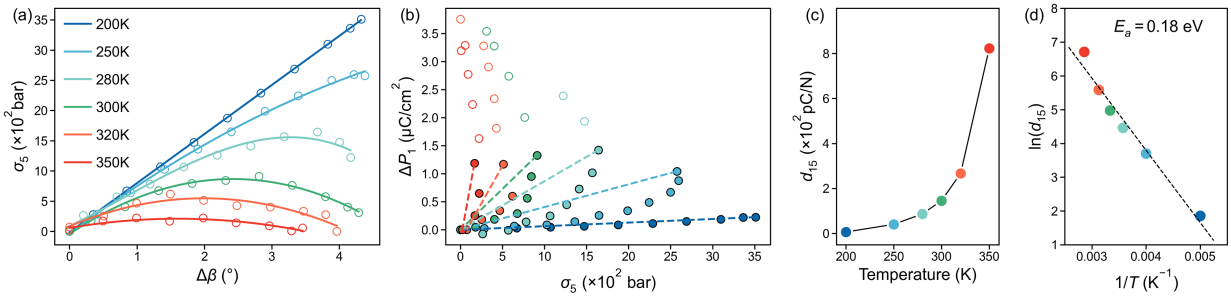

FIG. 3. Temperature-dependent piezoelectric response of TMCM-$CdCl_3$. (a) Shear stress-strain curves obtained from MD simulations at temperatures ranging from 200 K to 350 K. Solid lines represent polynomial fits to the simulation data. (b) Corresponding polarization change ΔP_1 as a function of applied shear stress σ_5 at each temperature. The piezoelectric coefficient d_{15} is extracted from the reversible response region, indicated by solid markers. (c) Temperature dependence of d_{15}. (d) Arrhenius plot of $\ln d_{15}$ versus $1/T$, with the dashed line indicating a linear fit. The slope yields an activation energy of $E_a = 0.18$ eV.

from stress-driven, symmetry-governed stochastic hopping of molecular dipoles by 120°. Crucially, only a small subset of local dipoles is activated, ensuring a reversible mechanical response. We find that the hopped dipoles tend to form transient quasi-one-dimensional clusters (see Fig. S15 [17]), resulting in a macroscopically small-angle rotation of the net polarization vector. As shown in Fig. 2(e), $\Delta\beta^t$ corresponds to a maximum rotation of global polarization by approximately 14°, significantly smaller than previously proposed values (56°) [14] and clearly distinct from the conventional polarization rotation mechanism [40]. Importantly, this behavior occurs without any phase transition, in contrast to earlier interpretations [12,14].

Because the stochastic hopping of molecular dipoles is inherently influenced by thermal fluctuations, we expect the piezoelectric coefficients to exhibit strong temperature dependence. We construct σ_5–$\Delta\beta$ curves across 200 K to 350 K [Fig. 3(a)], from which the corresponding ΔP_1–σ_5 curves are derived [Fig. 3(b)]. At each temperature, the shear piezoelectric coefficient d_{15} is estimated as $d_{15} = \Delta P_1^t/\sigma_5^t$. As expected, d_{15} increases dramatically with temperature, from 6 pC/N at 200 K to 823 pC/N at 350 K. We find that this trend follows Arrhenius behavior: plotting $\ln d_{15}$ against $1/T$ yields a linear relationship. The slope corresponds to an activation energy (E_a) of 0.18 eV, matching the rotational barrier of a single $TMCM^+$ cation at 300 K obtained from enhanced sampling MD (see Fig. S16 [17]). We note that our MD simulations predict $d_{35} > d_{15}$ at 200 K, consistent with previous zero-Kelvin DFT results using the Perdew-Burke-Ernzerhof functional [14] as well as with our own calculations incorporating Grimme's D3 dispersion corrections (see Fig. S17 [17]).

The turnover in the stress-strain curve beyond $\Delta\beta^t$ reflects a stress-relaxation process [Fig. 2(a)] conceptually analogous to plastic deformation in metals. MD simulations reveal that this relaxation occurs through the dipole hopping, which plays a similar role to dislocation defects in metals that enable plasticity (see Fig. S18 [17]) [41]. This analogy motivates further exploration of the mechanical response of TMCM-$CdCl_3$ under large shear stress or strain, which could define the material's operational limit.

Figure 4(a) presents the full stress-strain curve, corresponding to an in-plane 180° ferroelastic switching event, as the monoclinic angle β is swept from 94.3° to 85.7°. This simulation serves as a computational analog of shear experiments performed at constant average strain rate, with each strain step using the final configuration of the previous step as its starting point. During this transition, the stress passes through a local minimum at $\beta \approx 90°$, corresponding to an intermediate state with a nearly isotropic in-plane dipole orientation distribution. Reaching the final $+P_1^s$ state from this high-entropy, disordered configuration requires reordering, which is kinetically hindered by a reduction in configurational entropy ($\Delta S < 0$). Overcoming this entropic barrier ($-T\Delta S > 0$) requires additional shear work, resulting in the elevated stress observed as the system reenters the low-entropy, ordered $+P_1^s$ state. This explains the asymmetry in the σ_5–$\Delta\beta$ curve. Once switching completes, molecular dipoles have exhausted all available hopping pathways. Further applied strain is accommodated solely by elastic lattice distortion, causing the stress to rise sharply and linearly, defining the "elastic region." In this P_1–σ_5 curve [Fig. 4(b)], we define another critical stress, σ_5^*, as the *minimum* stress required to complete the ferroelastic switching process. Assuming a quasiequilibrium process driven by σ_5^*, the system eventually equilibrates in the elastic region when the internal stress balances σ_5^*. This gives an effective piezoelectric coefficient associated with ferroelastic switching: $d_{15}^* = \Delta P_1^*/\sigma_5^* = 793$ pC/N.

However, this ultrahigh response is a one-time effect under unipolar stress. After unloading, the system relaxes to the $+P_1^s$ state (Fig. 4 inset). Subsequent stress in the same direction will operate only within the elastic regime, yielding negligible piezoelectric response. This irreversible ferroelastic switching thus acts as a fatigue mechanism, explaining how a sample could be rendered piezoelectrically inactive if driven beyond its reversible limit. That said, if ferroelastic switching could be made reversible,

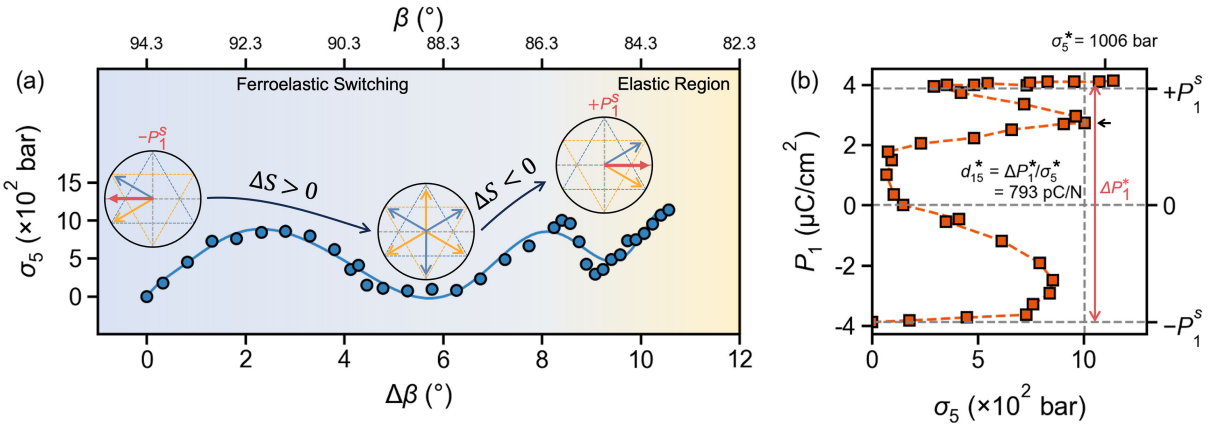

FIG. 4. Ferroelastic switching driven by large shear stress. (a) Shear stress-strain curve corresponding to a full reversal of in-plane polarization ($-P_1^s \rightarrow +P_1^s$) driven by shear stress σ_5. Insets illustrate the in-plane orientations of molecular dipoles during the switching process. The stress exhibits a characteristic increase followed by a decrease, reminiscent of the plastic deformation behavior observed in metals. An intermediate state near $\beta \approx 90°$ shows a nearly isotropic distribution of in-plane dipoles. Upon completing the switching, the system enters an elastic regime where stress increases linearly with strain. The stress-strain curve for the reverse process $+P_1^s \rightarrow -P_1^s$ closely matches that in (a) (see Fig. S19 [17]). (b) Hysteresis loop showing the relationship between shear stress σ_5 and polarization P_1 during the switching process in (a). The maximum stress σ_5^* defines the threshold required to complete the ferroelastic switching. The corresponding maximum (irreversible) piezoelectric response is estimated as $d_{15}^* = \Delta P_1^*/\sigma_5^*$.

for example, through domain wall engineering, the piezoelectric response of TMCM-$CdCl_3$ could be enhanced by over 350%. This is consistent with recent experiments on TMCM-$CdCl_3$ thin films, where substrate-induced strain generated periodic domain patterns and significantly boosted the piezoelectric response at domain walls [42].

In summary, using finite-temperature, large-scale molecular dynamics simulations enabled by a first-principles-based machine-learning force field, we have developed a robust approach to compute the full piezoelectric tensor for organic-inorganic hybrid perovskites represented by TMCM-$CdCl_3$. This method captures key anharmonic effects associated with the thermally driven order-disorder behavior of molecular dipoles. We demonstrate that the giant piezoelectric response is dominated by intrinsic components like d_{15} and d_{11}, which arise from stochastic in-plane hopping of molecular dipoles. The Arrhenius temperature dependence of the coefficients further highlights the thermally activated nature. The mechanism of discrete, localized hopping is fundamentally different from the continuous, bulk polarization rotation that drives the response in conventional piezoceramics [40,43]. Importantly, the reversibility of the response depends on limited dipole activation, while in-plane 180° ferroelastic switching serves as both a potential fatigue mechanism and a pathway for further enhancement if made reversible. Our Letter underscores the potential of engineering host-guest halogen bonds to tailor the rotational energy landscape of molecular dipoles for improved performance.

Acknowledgments—We acknowledge support from the National Natural Science Foundation of China (92370104) and Zhejiang Provincial Natural Science Foundation of China (LR25A040004). The computational resource is provided by Westlake HPC Center.

Data availability—The data that support the findings of this article are openly available [39].

[1] F. Li, B. Wang, X. Gao, D. Damjanovic, L.-Q. Chen, and S. Zhang, Ferroelectric materials toward next-generation electromechanical technologies, Science **389**, eadn4926 (2025).

[2] M. Acosta, N. Novak, V. Rojas, S. Patel, R. Vaish, J. Koruza, J. Rossetti, G. A. Rossetti, Jr., and J. Rödel, $BaTiO_3$-based piezoelectrics: Fundamentals, current status, and perspectives, Appl. Phys. Rev. **4**, 041305 (2017).

[3] M. Höfling, X. Zhou, L. M. Riemer, E. Bruder, B. Liu, L. Zhou, P. B. Groszewicz, F. Zhuo, B.-X. Xu, K. Durst, X. Tan, D. Damjanovic, J. Koruza, and J. Rödel, Control of polarization in bulk ferroelectrics by mechanical dislocation imprint, Science **372**, 961 (2021).

[4] B. Jaffe, R. Roth, and S. Marzullo, Piezoelectric properties of lead zirconate-lead titanate solid-solution ceramics, J. Appl. Phys. **25**, 809 (1954).

[5] S. Zhang, F. Li, X. Jiang, J. Kim, J. Luo, and X. Geng, Advantages and challenges of relaxor-$PbTiO_3$ ferroelectric crystals for electroacoustic transducers—A review, Prog. Mater. Sci. **68**, 1 (2015).

[6] J. Li, W. Qu, J. Daniels, H. Wu, L. Liu, J. Wu, M. Wang, S. Checchia, S. Yang, H. Lei, R. Lv, Y. Zhang, D. Wang, X. Li, X. Ding, J. Sun, Z. Xu, Y. Chang, S. Zhang, and F. Li, Lead zirconate titanate ceramics with aligned crystallite grains, Science **380**, 87 (2023).

[7] A. J. Lovinger, Ferroelectric polymers, Science **220**, 1115 (1983).

[8] Y. Liu and Q. Wang, Ferroelectric polymers exhibiting negative longitudinal piezoelectric coefficient: Progress and prospects, Adv. Sci. **7**, 1902468 (2020).

[9] Z. Sun, A. Zeb, S. Liu, C. Ji, T. Khan, L. Li, M. Hong, and J. Luo, Exploring a lead-free semiconducting hybrid ferroelectric with a zero-dimensional perovskite-like structure, Angew. Chem., Int. Ed. **55**, 11854 (2016).

[10] H.-Y. Ye, Y.-Y. Tang, P.-F. Li, W.-Q. Liao, J.-X. Gao, X.-N. Hua, H. Cai, P.-P. Shi, Y.-M. You, and R.-G. Xiong, Metal-free three-dimensional perovskite ferroelectrics, Science **361**, 151 (2018).

[11] W.-Q. Liao, D. Zhao, Y.-Y. Tang, Y. Zhang, P.-F. Li, P.-P. Shi, X.-G. Chen, Y.-M. You, and R.-G. Xiong, A molecular perovskite solid solution with piezoelectricity stronger than lead zirconate titanate, Science **363**, 1206 (2019).

[12] Y.-M. You, W.-Q. Liao, D. Zhao, H.-Y. Ye, Y. Zhang, Q. Zhou, X. Niu, J. Wang, P.-F. Li, D.-W. Fu, Z. Wang, S. Gao, K. Yang, J.-M. Liu, J. Li, Y. Yan, and R.-G. Xiong, An organic-inorganic perovskite ferroelectric with large piezoelectric response, Science **357**, 306 (2017).

[13] M. Zgonik, P. Bernasconi, M. Duelli, R. Schlesser, P. Günter, M. H. Garrett, D. Rytz, Y. Zhu, and X. Wu, Dielectric, elastic, piezoelectric, electro-optic, and elasto-optic tensors of $BaTiO_3$ crystals, Phys. Rev. B **50**, 5941 (1994).

[14] P. S. Ghosh, S. Lisenkov, and I. Ponomareva, Phase switching as the origin of large piezoelectric response in organic-inorganic perovskites: A first-principles study, Phys. Rev. Lett. **125**, 207601 (2020).

[15] Y. Lin, C. Chai, Z. Liu, J. Wang, S. Jin, Y. Yang, Y. Gao, M. Hao, X. Li, Y. Hou, X. Ma, B. Wang, Z. Wang, Y. Kan, J. Zheng, Y. Bai, Y. Chen, J. Sun, T. Zhao, J. Y. Law, V. Franco, F. Hu, and B. Shen, Large low-field-driven electrocaloric effect in organic-inorganic hybrid TMCM-$CdCl_3$, Nat. Commun. **16**, 4009 (2025).

[16] K. Tolborg and A. Walsh, Models of orientational disorder in hybrid organic–inorganic piezoelectric materials, J. Mater. Chem. C **11**, 8885 (2023).

[17] See Supplemental Material at http://link.aps.org/supplemental/10.1103/vxdj-zpy3, which includes Refs. [18–35], for computation methods, validation of the simulation protocol, and additional discussions.

[18] M. Chen, G. Guo, and L. He, Systematically improvable optimized atomic basis sets for *ab initio* calculations, J. Phys. Condens. Matter **22**, 445501 (2010).

[19] P. Li, X. Liu, M. Chen, P. Lin, X. Ren, L. Lin, C. Yang, and L. He, Large-scale *ab initio* simulations based on systematically improvable atomic basis, Comput. Mater. Sci. **112**, 503 (2016).

[20] P. Lin, X. Ren, X. Liu, and L. He, *Ab initio* electronic structure calculations based on numerical atomic orbitals: Basic fomalisms and recent progresses, Comput. Mol. Sci. **14**, e1687 (2024).

[21] M. Schlipf and F. Gygi, Optimization algorithm for the generation of ONCV pseudopotentials, Comput. Phys. Commun. **196**, 36 (2015).

[22] J. P. Perdew, K. Burke, and M. Ernzerhof, Generalized gradient approximation made simple, Phys. Rev. Lett. **77**, 3865 (1996).

[23] S. Grimme, J. Antony, S. Ehrlich, and H. Krieg, A consistent and accurate *ab initio* parametrization of density functional dispersion correction (DFT-D) for the 94 elements H-Pu, J. Chem. Phys. **132**, 154104 (2010).

[24] P. Ghosh, J. Doherty, S. Lisenkov, and I. Ponomareva, Tunability of structure, polarization, and band gap of high T_c organic–inorganic ferroelectrics by hydrostatic pressure: First-principles study, J. Phys. Chem. C **125**, 16296 (2021).

[25] J. Zeng *et al.*, DeePMD-kit v2: A software package for deep potential models, J. Chem. Phys. **159**, 054801 (2023).

[26] Y. Zhang, H. Wang, W. Chen, J. Zeng, L. Zhang, H. Wang, and W. E, DP-GEN: A concurrent learning platform for the generation of reliable deep learning based potential energy models, Comput. Phys. Commun. **253**, 107206 (2020).

[27] J. Wu, Y. Zhang, L. Zhang, and S. Liu, Deep learning of accurate force field of ferroelectric HfO_2, Phys. Rev. B **103**, 024108 (2021).

[28] J. Wu, J. Yang, L. Ma, L. Zhang, and S. Liu, Modular development of deep potential for complex solid solutions, Phys. Rev. B **107**, 144102 (2023).

[29] G. A. Tribello, M. Bonomi, D. Branduardi, C. Camilloni, and G. Bussi, Plumed 2: New feathers for an old bird, Comput. Phys. Commun. **185**, 604 (2014).

[30] A. Laio and M. Parrinello, Escaping free-energy minima, Proc. Natl. Acad. Sci. U.S.A. **99**, 12562 (2002).

[31] P. Xie, Y. Chen, W. E, and R. Car, Thermal disorder and phonon softening in the ferroelectric phase transition of lead titanate, Phys. Rev. B **111**, 094113 (2025).

[32] A. P. Thompson, H. M. Aktulga, R. Berger, D. S. Bolintineanu, W. M. Brown, P. S. Crozier, P. J. in 't Veld, A. Kohlmeyer, S. G. Moore, T. D. Nguyen, R. Shan, M. J. Stevens, J. Tranchida, C. Trott, and S. J. Plimpton, LAMMPS—A flexible simulation tool for particle-based materials modeling at the atomic, meso, and continuum scales, Comput. Phys. Commun. **271**, 108171 (2022).

[33] J. Shi, I. Grinberg, X. Wang, and A. M. Rappe, Atomic sublattice decomposition of piezoelectric response in tetragonal $PbTiO_3$, $BaTiO_3$ and $KNbO_3$, Phys. Rev. B **89**, 094105 (2014).

[34] S. Liu, F. Zheng, I. Grinberg, and A. M. Rappe, Photoferroelectric atomic sublattice decomposition of piezoelectricand photopiezoelectric properties of organometal halide perovskites, J. Phys. Chem. Lett. **7**, 1460 (2016).

[35] Z.-J. Feng, Y.-A. Xiong, W.-C. Sun, T.-T. Sha, J. Yao, Q. Pan, H. Hu, S. Dong, R.-G. Xiong, and Y.-M. You, First observation of negative capacitance in molecular ferroelectric thin films, Adv. Mater. **36**, 2307518 (2024).

[36] E. D. Sødahl, J. Walker, and K. Berland, Piezoelectric response of plastic ionic molecular crystals: Role of molecular rotation, Cryst. Growth Des. **23**, 729 (2023).

[37] L. Zhang, J. Han, H. Wang, R. Car, and W. E, Deep potential molecular dynamics: A scalable model with the accuracy of quantum mechanics, Phys. Rev. Lett. **120**, 143001 (2018).

[38] L. Zhang, J. Han, H. Wang, W. A. Saidi, R. Car, and E. Weinan, End-to-end symmetry preserving inter-atomic potential energy model for finite and extended systems, in *Proceedings of the 32nd International Conference on Neural Information Processing Systems, NIPS'18* (Curran Associates Inc., Red Hook, NY, USA, 2018), pp. 4441–4451.

[39] Available online at https://github.com/MoseyQAQ/TMCM-CdCl3-Piezoelectricity.

[40] H. Fu and R. E. Cohen, Polarization rotation mechanism for ultrahigh electromechanical response in single-crystal piezoelectrics, Nature (London) **403**, 281 (2000).

[41] N. Hansen and C. Barlow, Plastic deformation of metals and alloys, in *Physical Metallurgy*, 5th ed., edited by D. E. Laughlin and K. Hono (Elsevier, Oxford, 2014), pp. 1681–1764.

[42] X.-J. Song, Y.-A. Xiong, R.-J. Zhou, X.-X. Cao, Z.-Y. Jing, H.-R. Ji, Z.-X. Gu, T.-T. Sha, R.-G. Xiong, and Y.-M. You, The first demonstration of strain-controlled periodic ferroelectric domains with superior piezoelectric response in molecular materials, Adv. Mater. **35**, 2211584 (2023).

[43] R. Guo, L. E. Cross, S.-E. Park, B. Noheda, B. Noheda, D. E. Cox, and G. Shirane, Origin of the high piezoelectric response in $PbZr_{1-x}Ti_xO_3$, Phys. Rev. Lett. **84**, 5423 (2000).